ELSEVIER

Journal of Alloys and Compounds 404–406 (2005) 377–383

Journal of ALLOYS AND COMPOUNDS

www.elsevier.com/locate/jallcom

Theoretical modeling of hydrogen storage materials: Prediction of structure, chemical bond character, and high-pressure behavior

P. Vajeeston*, P. Ravindran, A. Kjekshus, H. Fjellvåg

Department of Chemistry, University of Oslo, Box 1033 Blindern, N-0315 Oslo, Norway

Received 29 July 2004; received in revised form 7 March 2005; accepted 14 March 2005
Available online 2 August 2005

Abstract

Density-functional theory (DFT) is a powerful tool to predict crystal structure, chemical bond character, and high-pressure behavior of materials. In this report, we show the application of DFT to study such properties for complex hydrides. The structural parameters for the experimentally known Li_3AlH_6 phase have been successfully reproduced within an accuracy of less than 1% and the crystal structure of $KAlH_4$ has been predicted. From examination of the density of state, we find that these materials have insulating behavior with a band gap of ~3.5 and 5.5 eV for Li_3AlH_6 and $KAlH_4$, respectively. From analyses of charge density, charge transfer, electron localization function, crystal orbital Hamilton, and Mulliken population we find that the interaction between Li/K and $[AlH_4]$/$[AlH_6]$ is essentially pure ionic, whereas within the $[AlH_4]$/$[AlH_6]$ unit the interaction is partially ionic and partially covalent. Even though these materials are very soft the Al–H interaction is relatively strong compared with the other interactions. Subject to external pressure the equilibrium structure of Li_3AlH_6 is unstable. We predicted that this compound undergoes three successive structural phase transitions under pressure: α to β at 18.64 GPa, β to γ at 28.85 GPa, and γ to ϵ at 68.79 GPa. $KAlH_4$ is stable and no pressure induced structural transitions were identified.

Keywords: Complex hydrides; Theoretical modeling; Structural stability; Chemical bond character; High-pressure behavior

1. Introduction

High capacity solid-state storage of hydrogen is becoming increasingly important for fuel cells, automotive, and electrical utility applications. Compared to liquid hydrogen one of the major drawbacks of known reversible metal hydrides applicable for hydrogen storage is their low gravimetric hydrogen content (expressed in wt.% of H in the material): MgH_2 (7.6%) and hydrides of Mg alloys (e.g., Mg_2NiH_4, 3.8%) represent in this respect the current optimum. However, for their use as storage materials a sufficient amount of heating (ca. 300 °C) is necessary for the desorption of the hydrogen. The disadvantage of the presently known, low- and medium-temperature reversible hydrides are the high costs for the intermetallic alloys suitable for the purpose ($LaNi_5H_6$, $TiFeH_2$), combined with their four to five times lower storage capacity (1.8%) compared with say MgH_2.

Alkali-metal-based aluminum hydrides, $AAlH_4$ (A = Li, Na, K) have been found to have a potential as viable modes for storing hydrogen at moderate temperatures and pressures. These hydrides have been demonstrated to have higher hydrogen storage capacity at moderate temperatures and lower cost than conventional intermetallic hydrides. However, a serious problem with these materials is poor kinetics and lacking reversibility with respect to hydrogen absorption/desorption. Bogdanovic and co-workers [1,2] have recently established that sodium aluminum hydrides, which were earlier considered in actual practice as irreversible with respect to hydrogen absorption/desorption, can be made reversible by doping with Ti. Efforts [3,4] have also been made to improve the hydrogen reversibility of $NaAlH_4$ by ball milling in combination with or without additives. In line with this, considerable interest is attached to the structural properties of the series ABH_4 and A_3BH_6 (A = alkali metal; B = B, Al, Ga) at ambient and higher pressures. In this article, we will demonstrate how density-functional theory (DFT) is used to predict unknown crystal structures, chem-

* Corresponding author. Tel.: +47 2285 5606; fax: +47 2285 5441.
E-mail address: ponniah.vajeeston@kjemi.uio.no (P. Vajeeston).

0925-8388/$ – see front matter © 2005 Elsevier B.V. All rights reserved.
doi:10.1016/j.jallcom.2005.03.109

ical bond characteristics, and high-pressure behavior of hydrides.

In the first part of the paper, we present the structural calculations for some complex hydrides. In the second part, we will consider the chemical bonding in selected hydrides with the help of partial density of states (DOS), crystal-orbital Hamilton population (COHP), charge density, charge difference, electron-localization function (ELF), and Mulliken population analysis. The third part deals with the structural stability of materials at high pressures based on total-energy studies.

2. Computational details

To predict the ground-state structure of Li_3AlH_6 and $KAlH_4$, we have used DFT [5] within the generalized-gradient approximation (GGA) [6], as implemented with a plane-wave basis in the Vienna ab initio simulations package (VASP) [7]. Results are obtained using projector-augmented plane-wave (PAW) [8] potentials provided with the VASP. The atoms are relaxed toward equilibrium until the Hellmann–Feynman forces are less than 10^{-3} eV/Å. Brillouin zone integration are performed with a Gaussian broadening of 0.1 eV during all relaxations. All calculations are performed with 512 and 600 **k** points for Li_3AlH_6 (Mg_3TeO_6-type structure) and $KAlH_4$ ($KGaH_4$-type structure), respectively, in the whole Brillouin zone with a 600 eV plane-wave cutoff. In order to avoid ambiguities regarding the free-energy results we have always used the same energy cutoff and a similar **k**-grid density for convergence for all structural variants tested. The present type of theoretical approach has recently been successfully applied [9–12] to reproduce structural properties of ambient- and high-pressure phases. The COHP is evaluated using the TBLMTO-47 package [13]. The Mulliken population analyses were made with the help of the CRYSTAL03 code in which we used 5-11G, 6-11G, 85-11G, and 86-511G basis sets for H, Li, Al, and K, respectively [14].

3. Structural prediction

Prediction and understanding of properties of materials (encompassing even not yet synthesized phases) by theoretical means is a valuable complement to the traditional experimental approach. Theoretical simulation of material properties before preparation and testing may save time, manpower, running costs, etc. Owing to the low X-ray scattering power of hydrogen, poor crystallinity, and the usual structural complexity of hydrides, these structures are often less characterized than other solids. For instance, this is the case for the (assumed technologically interesting materials) alkali boron, alkali aluminum and alkali gallium tetrahydrides, among which only a few is structurally well characterized. In the present section, we are going to show how DFT calculations can be used to predict the structures of the experimentally characterized Li_3AlH_6 (Fig. 1) and uncharacterized $KAlH_4$ compounds.

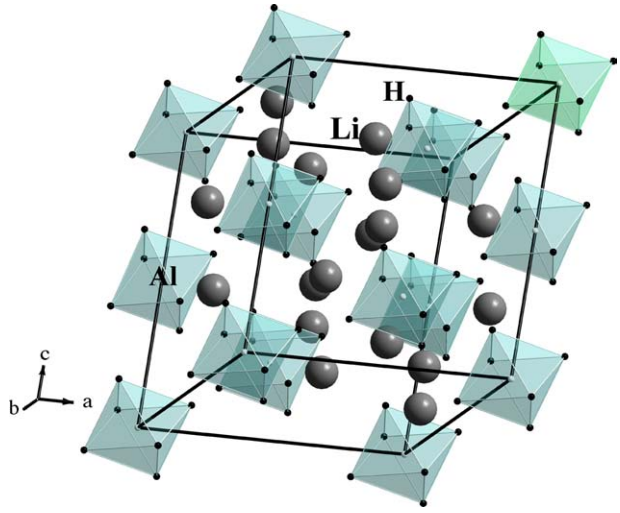

Fig. 1. The Mg_3TeO_6-type crystal structure of α-Li_3AlH_6. Locations of H and Li are shown (and labeled) in the illustration. Al is located at the center of the octahedra.

3.1. The crystal structure of Li_3AlH_6

The crystal structure of Li_3AlH_6 has up to recently not been completely revealed and several structure models have been proposed with possible monoclinic ($P2_1/c$, $P2_1/m$, $C2/m$, Cm, or $C2$) and rhombohedral ($R3$, $R\bar{3}$, $R3m$, or $R\bar{3}m$) space groups [15–17]. There has been no theoretical attempt to explore the crystal and electronic structures of this compound. However, a fresh experimental study by Brinks and Hauback [18] with combined synchrotron X-ray and neutron diffraction has shown that Li_3AlH_6 crystallizes in space group $R\bar{3}$.

Twenty-one closely related potential structure types were considered for the theoretical simulation. The involved structure types are: Li_3AlF_6, B_3BiO_6, Na_3AlH_6, Na_3AlF_6, Na_3CrCl_6, Mg_3TeO_6, K_3MoF_6, K_3TlF_6, Fe_3BO_6, Cu_3TeO_6, Cu_3WO_6, Rb_3TlF_6, Nb_3BaO_6, Nb_3VS_6, I_3AsF_6, Hg_3SO_6, Hg_3NbF_6, Hg_3TeO_6, Pb_3SO_6, Er_3GaS_6, and U_3ScS_6 [19]. The calculated total energy versus cell-volume curves for the 14 most relevant structural arrangements (the others fall at higher total energy) are shown in Fig. 2. Among them the Mg_3TeO_6-type arrangement (hereafter designated α-Li_3AlH_6; Fig. 2 and Table 1) is found to lead to the lowest total energy, consistent with the recent experimental findings [18]. The calculated unit-cell dimensions and positional parameters at 0 K and ambient pressure are in good agreement with the room-temperature experimental findings [the calculated a is within 0.3% of the experimental value whereas the slight underestimation (0.6%) in c is typical for the agreement obtained by DFT calculations]. It is interesting to note that the β (Cu_3TeO_6-type) and γ-(Li_3AlF_6-type) modifications

Table 1
Optimized structural parameters for Li_3AlH_6 and $KAlH_4$ at 0 K and ambient pressure

Compound (structure type; space group)	Unit-cell dimension (Å)	Positional parameters	B_0 (GPa)
α-Li_3AlH_6 (Mg_3TeO_6; $R\bar{3}$)	$a = 8.0487$ (8.0712)[a] $c = 9.4532$ (9.5130)[a]	Li (18*f*): 0.9334, 0.2196, 0.2804 (0.9576, 0.2260, 0.2911)[a]; Al1 (3*a*): 0.0, 0.0, 0.0; Al2 (3*b*): 0.0, 0.0, 1/2; H1 (18*f*): 0.8307, 0.8264, 0.0986 (0.8333, 0.8057, 0.1007)[a]; H2 (18*f*): 0.1372, 0.2014 , 0.3978 (0.1582, 0.1820, 0.3900)[a]	35.75
$KAlH_4$ ($KGaH_4$; *Pnma*)	$a = 8.8249$ (8.8140)[b] $b = 5.8590$ (5.8190)[b] $c = 7.3872$ (7.3310)[b]	K (4*c*): 0.1778, 1/4, 0.1621 Al (4*c*): 0.5663, 1/4, 0.8184 H1 (4*c*): 0.4034, 1/4, 0.9184 H2 (4*c*): 0.7055, 1/4, 0.9623 H3 (8*d*): 0.4194, 0.9810, 0.3127	10.34

[a] Experimental value at 295 K and ambient pressure from Ref. [18].
[b] Experimental value at 295 K and ambient pressure from Ref. [20].

are energetically very close to α-Li_3AlH_6. This indicates that synthesis under appropriate pressure and temperature conditions may be able to stabilize the β and γ modifications as metastable phases.

The α-Li_3AlH_6 structure consists of isolated $[AlH_6]^{3-}$ octahedra. Each Li atom is connected to two corners and two edges of these $[AlH_6]^{3-}$ octahedra. There are two crystallographically different Al sites, both with equal Al–H distances within each octahedron, but with slightly deviating angles from the ideal 90° value. Al has eight nearest Al neighbors, in a cubic arrangement, and six more distanced neighbors placed about the faces of the cube.

3.2. Crystal structure of $KAlH_4$

Recent experimental evidence shows that reversible hydrogen absorption/desorption proceeds smoothly in $KAlH_4$ without introduction of a catalyst [21]. $KAlH_4$ is thus different from $LiAlH_4$ and $NaAlH_4$, which have to be doped with a transition-metal catalyst material to obtain absorption/desorption reversibility and kinetics. Hence, $KAlH_4$ has now received considerable attention among the alkali-metal aluminum hydrides. The crystal structures of $LiAlH_4$ and $NaAlH_4$ are well known, whereas a more complete structural description for $KAlH_4$ has not yet been reported, the present experimental structural knowledge being limited to unit-cell dimensions at room temperature [20].

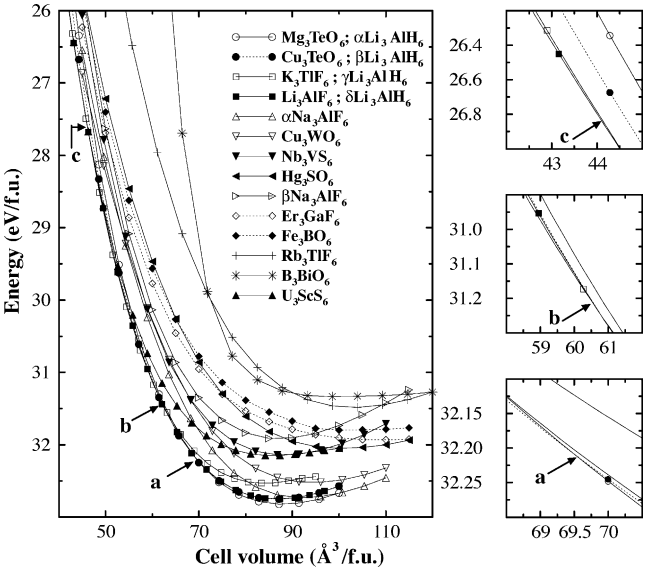

Fig. 2. Structural competition between different possible modifications of Li_3AlH_6. Magnified versions around structural transition points are shown on the right-hand side of the illustration. Arrows mark the cross-over points in the total-energy curves between different phases. Transition pressures are calculated from the Gibbs free-energy curves.

Among the seven tested possible structural variants (structure types specified in Refs. [9,11,22]), the orthorhombic $KGaH_4$-type arrangement (Table 1) is seen to have the lowest total energy with unit-cell dimensions $a = 8.824$, $b = 5.859$, $c = 7.387$ Å at 0 K and ambient pressure. However, the tetragonal α-$NaAlH_4$-type phase is energetically very close to the $KGaH_4$-type ground-state phase. This indicates that syntheses under appropriate pressure and temperature conditions may be able to stabilize the α-$NaAlH_4$-type arrangement as a metastable state. The $KGaH_4$- and α-$NaAlH_4$-type variants of $KAlH_4$ have not only a small total-energy difference, but also their equilibrium volumes are similar ($V_0 = 96.15$ and 93.95 Å^3/f.u., respectively). The calculated cell volume for the $KGaH_4$-type ground-state variant is in very good agreement with the observations, remembering that the calculations refer to 0 K and the experimental values to room temperature. A recent powder neutron diffraction study [23] on $KAlH_4$ confirms our predictions and finds also experimental positional parameters in good agreement with the calculated values in Table 1.

$KAlH_4$ is isostructural and isoelectronic with $KGaH_4$ whereas other isoelectronic compounds like $NaAlH_4$ and $NaGaH_4$ take rather different crystal structures. The $KAlH_4$ ground-state structure consists of slightly distorted $[AlH_4]^-$ tetrahedra which are separated by intervening K^+ cations. The interatomic Al–H distance within the $[AlH_4]^-$ tetrahedra varies only by 3% and the bond length is as expected for an anionic complex of Al and H [24]. Each K is surrounded by 12 H atoms at distances varying between 2.684 and 3.561 Å. The α-$NaAlH_4$-type structures of the proposed metastable modification of $KAlH_4$ also comprises tetrahedral $[AlH_4]^-$ anions and K^+ cations, but in a different mutual arrangement (see Fig. 1a in Ref. [9]).

4. Chemical bonding

The chemical bonding in materials becomes complicated when the number of distinguishable constituent increases. For binary compounds one can easily assess the degree of ionic character from electronegativities using Gordy's approximation [25]. For ternary and quaternary phases it is harder to estimate the ionic character. When we consider hydrides, it is even more complicated than for other compounds, because of the small size of the hydrogen atom and its only one valence electron. It is important to understand the bonding character of materials in detail in order to explain why some materials have peculiar properties compared to other materials in say, a certain series. For example, the $RNiInH_{1.333}$ (R = La, Ce, Pr, Nd) series of compounds violates the so-called "2 Å rule" for metal hydrides with the H–H separations of ~1.6 Å [26]. The reason appears to be that the presence of strong interaction between the transition metal (Ni) and hydrogen prohibits the electrons at the hydrogen atoms from participation in repulsive interaction between two closely arranged H atoms. Moreover, the R–R interaction also shields the repulsive interaction between the H atoms [27–29]. The bonding features of the $RNiInH_{1.333}$ series have been explained with the help of partial density of states (PDOS), charge-density distribution, charge difference plot, ELF, and COHP analysis [27]. Our experience with this series of hydrides shows that several theoretical methods are needed in order to characterize the bonding correctly in order not to end up with wrong conclusions [27–29].

In the present study, we try to explore the bonding in $KAlH_4$ and Li_3AlH_6. We believe that a similar type of bonding may be present in the AMH_4 (A = Li, Na, K, Rb, Cs; M = B, Al, Ga) and A_3AlH_6 (A = Li, Na, K) families, because all these compounds have almost similar charge-density distribution, DOS, and ELF. The calculated DOS of $KAlH_4$ and Li_3AlH_6 and partial DOS of $KAlH_4$ are displayed in Fig. 3. From the total DOSs, it is clear that $KAlH_4$ and Li_3AlH_6 are to be classified as insulators with a band gap of ca. 3.5 and 5.5 eV for Li_3AlH_6 and $KAlH_4$, respectively, which is close to the band gaps in other technologically interesting hydrides, viz. MgH_2 (4.3 eV [10]), $LiAlH_4$ (4.8 eV [11]), and $NaAlH_4$ (5.0 eV [9]). The PDOSs for $KAlH_4$ and Li_3AlH_6 show close similarities, hence we present only the DOS for $KAlH_4$. The site-projected DOSs of K and Al show that the lower peak in the total DOS mainly originates from Al-s states with small contributions from H-s, K-s, and K-p states, whereas the upper peak comprises contributions from H-s, Al-p, K-s, and K-p states. The Al-s and Al-p states are energetically well separated in the valence band (VB) whereas the K-s and K-p states are energetically degenerated throughout the VB. Al-p and H-s states are energetically degenerated in corresponding energy regions in the VB which is a favorable situation for formation of covalent bonds within the anionic $[AlH_4]^-$ complex. From an electronegativity point of view, the bonding Al–H interaction is also expected to be of a largely covalent nature, whereas the K–H, Li–H interaction should be ionic.

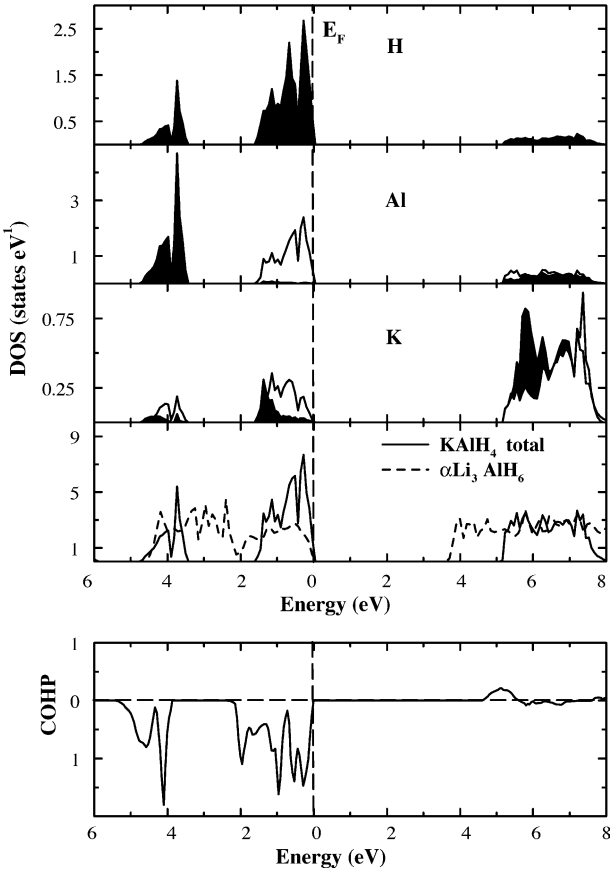

Fig. 3. *Upper panels*: Calculated total DOS for $KAlH_4$ and α-Li_3AlH_6 and site-projected DOSs for $KAlH_4$. The Fermi level is set at zero energy and marked by the vertical dotted line; *s* states are shaded. *Lower panels*: Calculated COHP between Al and H in $KAlH_4$.

Fig. 4a shows the calculated valence-charge density for $KAlH_4$. At the K, Al, and H sites; high amounts of charge density reside in the immediate vicinity of the nuclei. However, there is an appreciable amount of electrons distributed between Al and H which is another indication of a significant degree of covalent-type interaction. The electron distribution between K and the $[AlH_4]$ unit is almost zero (charge depletion; see Fig. 4b), viz. an indication of ionic-type interaction between K and $[AlH_4]$. The calculated charge-transfer plot (charge-density difference between the solid and overlapping free atomic orbitals) moreover clearly show that charges are depleted from the K and Al sites and transferred to the H sites, viz. the interaction between the K/Al and H has ionic components. For a purely ionic case one can expect a perfect spherically symmetric charge depletion as observed at the K site. The charge depletion at the Al site is not spherically symmetric in the two cases under consideration.

Then, we turn to ELF which is defined in the range 0–1; and high values reflect covalent bonds or lone electron pairs. The calculated ELF for $KAlH_4$ at the H sites is not spherically

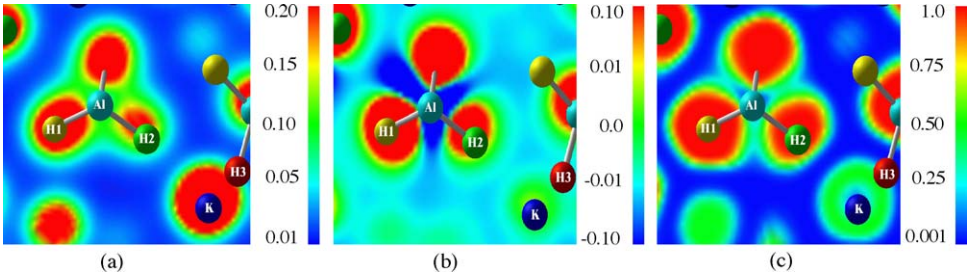

Fig. 4. Calculated (a) valence electron charge density, (b) charge transfer, and (c) ELF for $KAlH_4$.

Table 2
Mulliken population analysis for Li_3AlH_6 and $KAlH_4$

Compound	Atom	MEC	Overlap population
Li_3AlH_6	Li	−1.008	
	Al	−2.032	−0.014 (Li–H)
	H	+0.844	0.105 (Al–H)
$KAlH_4$	K	−1.098	
	Al	−1.880	−0.015 (K–H)
	H	+0.749	0.171 (Al–H)

Mulliken effective charge (difference between the number of electrons of the atom concerned and the corresponding Mulliken charge; MEC) and Mulliken overlap population in units of *e*.

symmetric indicating that the electrons are polarized toward the Al site (Fig. 4c). A similar type of ELF is found in molecular C_2H_6 and C_2H_4, where the interaction between C and H is covalent [30]. Hence, one infers directional, covalent-type bonding between Al and H in $KAlH_4$ and α-Li_3AlH_6. The calculated integrated COHP (which is a tool to gauge the bond strength between involved atoms) indicates that the interaction, between Al and H is the strongest (integrated COHP value −2.39 eV) compared to other interactions, and the estimated bond strength vary in the sequence Al–H > K/Li–H > K/Li–Al > H–H. In order to have some kind of quantitative picture of the charge-transfer effect we also made the Mulliken population (a means to quantify the amount of electrons on a given atom in a solid) analyses [31]. The Mulliken effective charges for Li, K, Al, and H in Li_3AlH_6 and $KAlH_4$ indicate (see Table 2) that the interaction between Li/K and $[AlH_6]$/$[AlH_4]$ is essentially pure ionic, viz. approximately one electron is transferred from Li or K to $[AlH_6]$ or $[AlH_4]$. There is a distinct overlap population present between Al and H within the $[AlH_6]$/$[AlH_4]$ units reflecting a covalent component of the Al–H chemical bond. The magnitude is smaller than found in a pure covalent bond, and the partial charges (around two electrons transferred from Al to H) imply a finite degree of ionic interaction.

5. Pressure induced structural transitions

In general, application of pressure will shorten the interatomic distances in a crystalline solid, and when the pressure exceeds a critical value a change in crystal structure may occur. The change in the structure brings about a change in the physical and chemical properties. In some cases high-pressure phases have peculiar properties compared with ambient-pressure phases. For example, in $LiAlH_4$ we note a huge pressure induced volume collapse (around 17%) at the α-to-β transition point [11]. Similarly, in BeH_2 there is an almost 26.4% reduction in volume at the phase-transition point from the equilibrium to a high-pressure phase [32].

Application of pressure transforms α-Li_3AlH_6 into the β modification (with Cu_3TeO_6-type structure) at 18.64 GPa [transition pressures are estimated from the pressure versus difference in Gibbs free energy (ΔG) curves; see Fig. 5]. The pressure induced α-to-β transition of Li_3AlH_6 (see Figs. 2 and 5) involves reconstructive rearrangements (viz. bonds are broken and re-established) of the atomic architecture. β-Li_3AlH_6 is stable in a fairly narrow pressure range and transform into γ-Li_3AlH_6 (K_3TlF_6-type) at 28.85 GPa and further to δ-Li_3AlH_6 (Li_3AlF_6-type) at 68.79 GPa. The α-, β-, and δ-Li_3AlH_6 phases have very similar equilibrium volumes (87.76, 86.74, and 86.78 $Å^3$/f.u., respectively) and the energy difference between them is also very small (see Fig. 2). This closeness in total energy suggests that the relative appearance of these modifications will be quite sensitive to, and easily affected by, external factors like temperature and remnant lattice stresses. The fact that the estimated volume difference is also small (Fig. 5) at the α-to-β phase-transition point suggests that α-Li_3AlH_6 has an efficiently packed structure; similarly, for the other modifications at the β-to-γ and γ-to-δ transitions (Fig. 5). As mentioned the volume discontinuity at the α-to-β transition point in $LiAlH_4$ [11] is ∼17%. The closeness in volume for the different Li_3AlH_6 modifications (at the transition pressures) should challenge the experimentalists to study this system carefully.

The calculated bulk moduli (B_0) for α-Li_3AlH_6 and $KAlH_4$ indicate that these materials are easily compressable solids. If we compare B_0 of diamond (432 GPa) with the studied phases (36 and 10 GPa for Li_3AlH_6 and $KAlH_4$, respectively) these compounds have 12–43 times smaller B_0 values. Hence one may have expected that the removal of H from these structures should have been quite easy. This is certainly not the case. The COHP study on these materials [33] shows that the interaction between Al and H is stronger (−2.62 to −3.44 eV) than the other interactions, and this appears to be a likely reason for the fact that these hydrides are

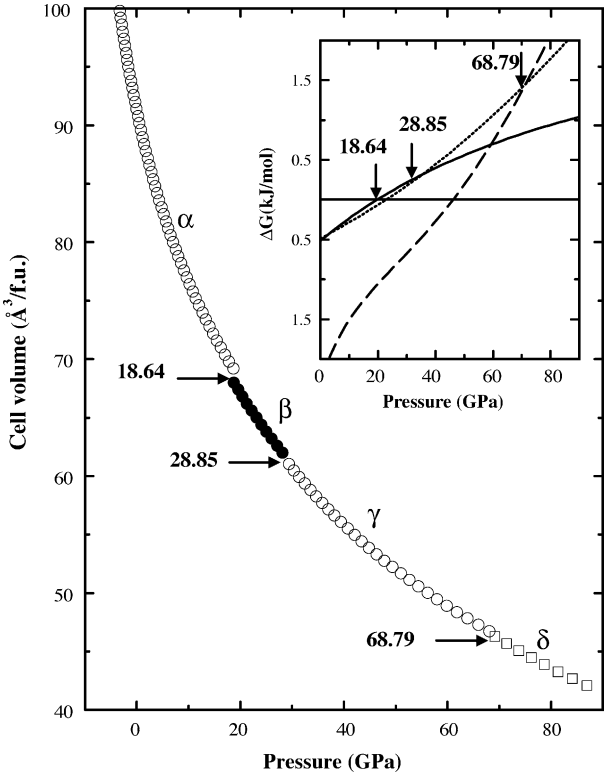

Fig. 5. Calculated pressure vs. cell-volume relation for Li_3AlH_6. The inset shows the stability of high-pressure phases of Li_3AlH_6 with respect to the equilibrium phase, transition pressures being marked by arrows at the corresponding transition points.

at the same time very soft and yet require much energy to remove all hydrogen.

6. Conclusions

In this study, we have successfully reproduced the structural properties of α-Li_3AlH_6, calculated positional and cell parameters being in very good agreement with experimental findings. We have predicted the crystal structure of $KAlH_4$. This ultimately indicates that the density-functional theory is a powerful tool to predict structural properties of materials at ambient and high pressures. One can formally treat $KAlH_4$ as a pure ionic compound but the detailed analysis on this compound shows that whereas the interaction between K and [AlH_4] is essentially pure ionic that between Al and H is mixture of ionic and covalent with the latter as the stronger component. This may be the possible reason why $KAlH_4$ (and Li_3AlH_6) has a high decomposition temperature. Due to close similarity in charge density and density of states distributions one can expect similar features in the whole $AAlH_4$ (A = Li, Na, K, Rb, Cs) family. From the high-pressure study on Li_3AlH_6 and $KAlH_4$, it is found that the ground-state structure of Li_3AlH_6 is not stable at higher pressure. Three high-pressure forms of Li_3AlH_6 have been identified. On the other hand, $KAlH_4$ is a stable compound which exhibit no pressure induced transitions.

Acknowledgements

P.V. and P.R. gratefully acknowledge Professor O.K. Andersen for being allowed to use his computer code and the Research Council of Norway for financial support. This work has also received support from the Research Council of Norway (Programme for Supercomputing) through a grant of computing time.

References

[1] B. Bogdanovic, M.J. Schwickardi, J. Alloys Compd. 253 (1997) 1.
[2] B. Bogdanovic, R.A. Brand, A. Marjanovic, M. Schwikardi, J. Tölle, J. Alloys Compd. 302 (2000) 36.
[3] A. Zaluska, L. Zaluski, J.O. Ström-Olsen, J. Alloys Compd. 298 (2000) 125.
[4] C.M. Jensen, K.J. Gross, Appl. Phys. a 72 (2001) 213.
[5] P. Hohenberg, W. Kohn, Phys. Rev. B 136 (1964) 864.
[6] J.P. Perdew, in: P. Ziesche, H. Eschrig (Eds.), Electronic Structure of Solids, Akademie Verlag, Berlin, 1991;
J.P. Perdew, K. Burke, Y. Wang, Phys. Rev. B 54 (1996) 16533;
J.P. Perdew, S. Burke, M. Ernzerhof, Phys. Rev. Lett. 77 (1996) 3865.
[7] G. Kresse, J. Hafner, Phys. Rev. B 47 (1993) R6726;
G. Kresse, J. Furthmuller, Comput. Mater. Sci. 6 (1996) 15.
[8] P.E. Blöchl, Phys. Rev. B 50 (1994) 17953;
G. Kresse, J. Joubert, Phys. Rev. B 59 (1999) 1758.
[9] P. Vajeeston, P. Ravindran, R. Vidya, A. Kjekshus, H. Fjellvåg, Appl. Phys. Lett. 82 (2003) 2257.
[10] P. Vajeeston, P. Ravindran, A. Kjekshus, H. Fjellvåg, Phys. Rev. Lett. 89 (2002) 175506.
[11] P. Vajeeston, P. Ravindran, R. Vidya, A. Kjekshus, H. Fjellvåg, Phys. Rev. B 68 (2003) 212101.
[12] U. Häussermann, H. Blomqvist, D. Noréus, Inorg. Chem. 41 (2002) 3684.
[13] G. Krier, O. Jepsen, A. Burkhardt, O.K. Andersen, Tight Binding LMTO-ASA Program Version 4.7, Stuttgart, Germany, 2000.
[14] http://www.crystal.unito.it/.
[15] V.P. Balema, V.K. Pecharsky, K.W. Dennis, J. Alloys Compd. 313 (2000) 69.
[16] R. Ehrlich, A. Young, G. Rice, J. Dvorak, P. Shapiro, H. Smith, J. Am. Chem. Soc. 88 (1966) 858.
[17] J. Mayet, S. Kovacevic, J. Tranchant, Bull. Soc. Chim. Fr. 2 (1973) 503.
[18] H.W. Brinks, B.C. Hauback, J. Alloys Compd. 354 (2003) 143.
[19] Inorganic Crystal Structure Database, Gmelin Institut, Germany, 2001/1.
[20] J.-P. Bastide, P. Claudy, J.-M. Letoffe, J.E. Hajri, Rev. Chim. Miner. 24 (1987) 248.
[21] H. Morioka, K. Kakizaki, S.C. Chung, A. Yamada, J. Alloys Compd. 353 (2003) 310.
[22] P. Vajeeston, P. Ravindran, H. Fjellvåg, A. Kjekshus, J. Alloys Compd. 363 (2003) 7.
[23] B.C. Hauback, H.W. Brinks, R. Blom, R.H. Heyn, H. Fjellvåg, unpublished.
[24] A.F. Wells, Structural Inorganic Chemistry, Clarendon, Oxford, 1987.
[25] W. Gordy, Discuss. Faraday Soc. 19 (1955) 23.
[26] V.A. Yartys, R.V. Denys, B.C. Hauback, H. Fjellvåg, I.I. Bulyk, A.B. Riabov, Y.M. Kalychak, J. Alloys Compd. 330–332 (2002) 132.

[27] P. Ravindran, P. Vajeeston, R. Vidya, A. Kjekshus, H. Fjellvåg, Phys. Rev. Lett. 89 (2002) 106403.
[28] P. Vajeeston, P. Ravindran, R. Vidya, H. Fjellvåg, A. Kjekshus, V.A. Yartys, Phys. Rev. B 67 (2003) 014101.
[29] P. Vajeeston, P. Ravindran, A. Kjekshus, H. Fjellvåg, Phys. Rev. B 70 (2004) 014107.
[30] A. Savin, A.D. Becke, J. Flad, R. Nesper, H. Preuss, H.G. von Schnering, Angew. Chem. Int. Ed. Engl. 30 (1991) 409;
A. Savin, O. Jepsen, J. Flad, O.K. Andersen, H. Preuss, H.G. von Schnering, Angew. Chem. Int. Ed. Engl. 31 (1992) 187.
[31] R.S. Mulliken, J. Chem. Phys. 23 (1955) 1833.
[32] P. Vajeeston, P. Ravindran, A. Kjekshus, H. Fjellvåg, Appl. Phys. Lett. 84 (2004) 34.
[33] P. Vajeeston, P. Ravindran, R. Vidya, A. Kjekshus, H. Fjellvåg, Cryst. Growth Des. 4 (2004) 471.